Composites Part B 267 (2023) 111005

Contents lists available at ScienceDirect

Composites Part B

journal homepage: www.elsevier.com/locate/compositesb

EGCG modified small intestine submucosa promotes wound healing through immunomodulation

Rong Nie [a,1], Qing-Yi Zhang [a,1], Jie Tan [a,d], Zi-Yuan Feng [a], Kai Huang [a], Ning Sheng [a], Yan-Lin Jiang [a,b], Yu-Ting Song [a], Chen-Yu Zou [a], Long-Mei Zhao [a], He-Xi Li [a], Rui Wang [a], Xing-Li Zhou [a], Juan-Juan Hu [a], Chen-Yu Wu [a], Jesse Li-Ling [a,b,c,**], Hui-Qi Xie [a,b,*]

[a] Department of Orthopedic Surgery and Orthopedic Research Institute, Laboratory of Stem Cell and Tissue Engineering, State Key Laboratory of Biotherapy, West China Hospital, Sichuan University, Chengdu, Sichuan, 610041, PR China
[b] Frontier Medical Center, Tianfu Jincheng Laboratory, Chengdu, Sichuan, 610212, PR China
[c] Department of Medical Genetics, West China Second Hospital, Sichuan University, Chengdu, Sichuan, 610041, PR China
[d] Department of Spine Surgery, Huazhong University of Science and Technology Union Shenzhen Hospital, Shenzhen, Guangdong, 518052, PR China

ARTICLE INFO

Handling Editor: Dr Hao Wang

Keywords:
Small intestinal submucosa
Epigallocatechin gallate
Immune microenvironment
Wound healing

ABSTRACT

Decellularized porcine small intestinal submucosa (SIS) has shown promising therapeutic efficacy as a functional wound dressing. Nevertheless, its limited anti-oxidative and immunomodulatory capacities have restricted its application for the treatment of complex skin wounds. Herein, epigallocatechin gallate (EGCG), a polyphenolic compound, was employed for the modification of the SIS to overcome such shortcomings. The EGCG-modified SIS (E-SIS) has shown excellent biocompatibility and improved hydrophilicity for cell adhesion. Notably, *in vitro* studies showed that the E-SIS could effectively alleviate oxidative stress and facilitate the M1-to-M2 phenotype transition of macrophages, thereby creating a favorable immune microenvironment for cell proliferation, migration, collagen synthesis as well as angiogenesis. A full-thickness skin defect model, combined with macrophage depletion, has further confirmed that the E-SIS could accelerate skin wound repair through immunomodulation *in vivo*. This suggested that the EGCG modification could provide a facile yet effective method to broaden the applications of the SIS for skin wound management.

1. Introduction

As the largest organ covering the body's surface, the skin serves a variety of functions including defense, sensing, endocrine and exocrine, temperature regulation as well as stress responding [1]. Even though the skin possesses an inherent self-repair capacity, when damage has exceeded a certain threshold, delayed and/or impaired wound healing may result, which is typically accompanied by hyperinflammation, impaired angiogenesis, and/or diffuse infection necessitating further intervention [2]. As estimated, over 50 billion dollars are spent annually on the treatment of skin wounds in the United States alone [3]. Consequently, it is crucial to investigate effective treatment methods for accelerating wound healing processes.

Wound healing progresses through a series of successive yet overlapping stages, which comprise hemostasis, inflammation, proliferation, and remodeling [4,5]. Notably, the substantial role of immune response that partakes throughout the whole healing process has garnered increased attention over the past decade. Upon injury, a robust inflammatory response is promptly initiated to eliminate pathogenic microorganisms and remove necrotic tissues. Subsequently, with the resolution of the inflammatory response, immune cells will transition to secreting various cytokines which can promote tissue repair and regeneration. A timely transition of the immune response is therefore essential for wound healing; conversely, excessive and/or prolonged inflammation may result in further tissue damage and intractable complications.

The macrophages are a major participant in immune response and have heterogeneous phenotypes [6]. They can be categorized into classically activated M1 and alternatively activated M2 types [7]. Generally, M1 macrophages, characterized by a de novo or increased

* Corresponding author. Jitaian Center, 17 Gaopeng Avenue, Hi-Tech District, Chengdu, Sichuan, 610041, PR China.
** Corresponding author. Jitaian Center, 17 Gaopeng Avenue, Hi-Tech District, Chengdu, Sichuan, 610041, PR China.
E-mail address: xiehuiqi@scu.edu.cn (H.-Q. Xie).
[1] Rong Nie and Qing-Yi Zhang have contributed equally to this work.

https://doi.org/10.1016/j.compositesb.2023.111005
Received 5 July 2023; Received in revised form 10 August 2023; Accepted 14 September 2023
Available online 20 September 2023
1359-8368/

iNOS and CD86, are recruited to the wound site within 24–48 h following the initial insult and may participate in both acute and chronic inflammation with a high phagocytic capacity and secret substantial amounts of inflammatory factors and reactive oxygen species [8]. By contrast, CD163 or CD206 positive M2 macrophages contain anti-inflammation factors and can promote healing, tissue remodeling and fibrosis though a regulatory and anti-inflammatory phenotype [9]. They are also highly phagocytic and can produce extracellular matrix (ECM) components and angiogenic factors. M1 and M2 macrophages play crucial roles at various stages of tissue repair. M1 macrophages will eliminate necrotic tissue and pathogenic microorganisms and initiate the early recruitment. M2 macrophages, by contrast, possess anti-inflammatory properties and can significantly contribute to the promotion of tissue repair. However, a disordered immune response may lead to continuous activation of M1 macrophages, causing a widespread of inflammatory responses and subsequent tissue damage. The failure to transit smoothly to M2 macrophages may hinder the pace of wound healing, leading to chronic non-healing wounds. Therefore, the regulation of a timely M1-to-M2 macrophage transition through the adjustment of scaffold physicochemical properties or administration of immunomodulatory drugs or bioactive components to create a favorite immune microenvironment, has been widely adopted as an effective strategy to expedite wound healing [2,10–13].

Decellularized ECM has proven to be a promising scaffold with excellent biocompatibility and bioactivities to accelerate tissue repair and regeneration. During the last decade, our group has developed a series of biomaterials based on decellularized porcine small intestinal submucosa (SIS). By effectively eliminating immunogenicity and preserving the integrity of the original structure and composition, these biomaterials have exhibited significant therapeutic efficacy and are applied for various clinical scenarios including the urethra, dura mater, bladder and digestive tract *etc*. [14–18]. Particularly, when the SIS patch is directly used as a dressing for skin wounds, it has displayed unique advantages over other forms of materials. On the one hand, the SIS can function as a barrier to prevent excessive evaporation of body fluids, ensuring a moist environment for the wound, which is essential to faster tissue regeneration and better wound healing outcomes. In addition, it can also prevent the intrusion of pathogenic microorganisms. Meanwhile, the SIS patches can be easily trimmed to fit the shapes of various wounds and directly adhere to the wound surface, reducing the secondary damage caused by frequent dressing changes. Besides, the rich functional groups in the SIS may facilitate the modification, allowing for further adjustments based on various needs. Therefore, the SIS patches may provide an ideal dressing for skin wounds, especially when the SIS is used as wound dressing. Nevertheless, as demonstrated by previous experiments, the SIS itself does not possess sufficient capability to handle the oxidative stress and immune microenvironment surrounding the wound sites [19]. How would augmenting the SIS with additional relevant functions may affect its therapeutic effects still requires more compelling evidence.

Epigallocatechin gallate (EGCG) is a green tea-derived polyphenolic compound. Owing to the abundant naphthol and resorcinol functional groups, the EGCG has inherently displayed remarkable properties for free radical scavenging, thereby presenting exemplary anti-oxidative and anti-inflammatory abilities. Moreover, the EGCG has shown remarkable crosslinking and adhesion capabilities across a variety of materials, irrespective of their types or morphology, and is therefore extensively employed for the modification of diverse materials [20]. In the field of biomedicine, the EGCG has confirmed to have a high affinity to diverse biomacromolecules through both covalent and non-covalent interactions, and can produce a range of unique pharmacological impacts by modulating signal transduction and/or enzymatic activities. Particularly, studies have demonstrated that the EGCG can effectively induce macrophage polarization towards the M2 type, which is essential to the tissue repair [21]. Herein, a novel EGCG-modified SIS patch (E-SIS) was developed for skin wound management and has displayed a more compact and dense topological structure, as well as enhanced hydrophilicity compared with the SIS (Fig. 1). Meanwhile, the E-SIS could effectively scavenge the ROS in the environment and promote the M1-to-M2 transition of the macrophages, thereby providing a beneficial environment for cell proliferation, migration, collagen synthesis, and angiogenesis to support wound healing. *In vivo,* full-thickness skin defect model of rats combined with macrophage depletion further revealed that the E-SIS could expedite wound healing through immunomodulation.

2. Materials and methods

2.1. Materials

Fresh porcine small intestines were purchased from slaughterhouses, while the EGCG was procured from Nanjing Kasaisi Medical Technology Co., Ltd. Lipopolysaccharide (LPS) was purchased from Solarbio (China). Live-dead staining was performed using materials from Sigma (USA), while the Cell Counting Kit-8 (CCK-8) was sourced from Dojindo Molecular Technologies (Japan). The ELISA kits utilized in this study were procured from Ruixinbio Quanzhou in China. Supplementary Materials contain information regarding the other reagents employed in this study.

2.2. Preparation of the E-SIS

The SIS was obtained as previously described [22]. Briefly, after thorough washing, the mucosa, serosa, and muscularis were removed by physical scraping. Thereafter, the SIS has undergone degreasing, and decellularization processes by sequentially immersing in methanol and chloroform mixture, 0.05% trypsin, 0.05% sodium dodecyl sulfate (SDS) for 12 h each. Finally, the SIS was thoroughly washed and lyophilized (LPHA 1–2 LD plus, CHRIST, Germany). For E-SIS preparation, the SIS was immersed in the EGCG solution with various concentrations (0.1%, 0.25%, 0.5%, 1%, and 2%, wt%) for 24 h. Similarly, after complete washing, the derived E-SIS was lyophilized for the subsequent experiments. Of note, pristine SIS was used as the control in the subsequent experiments.

2.3. Characterization of the E-SIS

The topological structure was analyzed by scanning electron microscope (SEM). Briefly, both sides of the SIS or E-SIS were individually coated with gold and subsequently scanned under an SEM (EVO 10, Carl Zeiss AG, Germany) at an accelerating voltage of 20.0 kV. Meanwhile, the crosslinking degree of the E-SIS was measured using an OPA method. Detailed operation methods are described in the Supplementary Materials. Fourier-transform infrared (FTIR, Nicolet iS50, Thermo Fisher Scientific, USA) test with a measurement range of 500–4000 cm^{-1} was also carried out to determine the physical characteristics of the E-SIS. In addition, to investigate the influence of EGCG on wettability, the water contact angle (WCA) was measured with a goniometer (DSA25, Kruss, Germany) at room temperature with three repetitions.

To evaluate the EGCG release characteristics, the E-SIS were cut into rectangles with a surface area of 3 cm^2 and immersed in 500 μL of PBS with continuous oscillation at 37 °C. At pre-scheduled time points, the supernatant was collected and replaced by an equal volume of fresh PBS. The content of EGCG was measured with a spectrophotometer (SYNERGY H1, BioTek, USA) at 275 nm [23]. The release profile of the EGCG was calculated according to the standard EGCG samples.

2.4. Cell culture

All cells used in the present study were obtained from the Cell Bank of the Chinese Academy of Sciences. Human umbilical vein endothelial cells (HUVECs) were cultured in Dulbecco's modified eagle medium

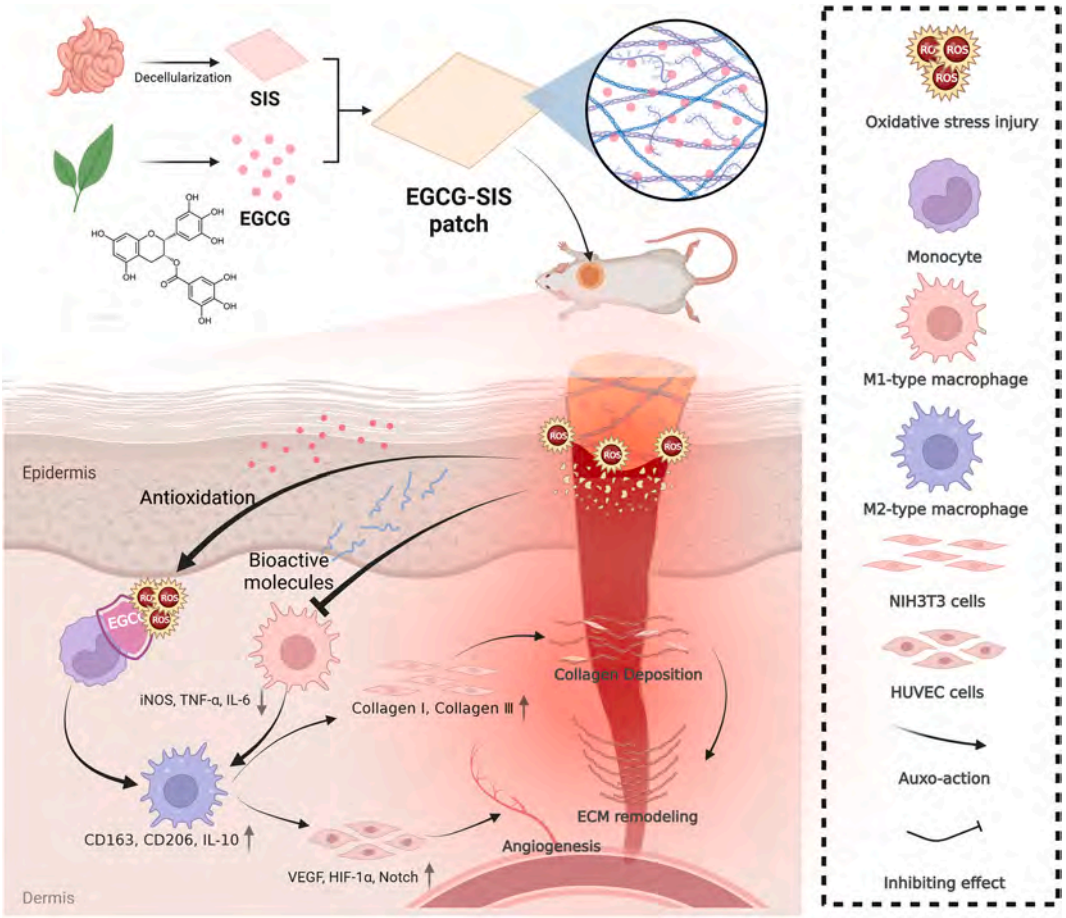

Fig. 1. Schematic overview of the E-SIS patches to accelerate wound healing by regulating macrophage polarization to M2 type as well as reducing oxidative stress to promote wound collagen deposition and angiogenesis.

(DMEM)/F12 supplemented with 10% fetal bovine serum (FBS) and 1% antibiotics. The NIH-3T3 cells were cultured in DMEM supplemented with 10% FBS and 1% antibiotics. The RAW264.7 cells were cultured in α-MEM supplemented with 10% heat-inactivated FBS and 1% antibiotics. All cells were cultured at 37 °C with saturated humidity. When confluence had reached 80%, cells were passaged at a ratio of 1 : 3.

2.5. Extraction and conditioned medium preparation

The extraction of the E-SIS was carried out in adherence to GB/T 16886.1/ISO 10993-1 guidelines. In brief, the extractions were procured by immersing the E-SIS in a comprehensive medium with a volume-to-surface ratio of 1 : 6 at 37 °C for 72 h.

For conditioned medium (CM), RAW264.7 cells were exposed to 100 ng/mL LPS for 6 h prior to culture with various patch extractions. After 48 h, the supernatant was collected, filtered, and mixed with the fresh complete medium of each cell with a ratio of 1 : 1 to obtain CM for subsequent use.

2.6. Evaluation of biocompatibility and cell adhesion

The cytocompatibility of the E-SIS patches was determined by live-dead staining and cell proliferation assay by following manufacturers' protocols. For live-dead staining, cell viability was observed under a confocal laser scanning microscope (CLSM, A1RMP + Nikon, Japan) after 48 h seeding onto various patches. For the cell proliferation assay, the cells were cultured with the extraction of various patches as described above. At pre-scheduled time points, cell proliferation was measured with a CCK-8. Cell relative survival rate (RSR) was calculated with: $RSR\ (\%) = OD_e / OD_{tn} \times 100\%$ (OD_e and OD_{tn} indicated the optical density of various patches groups and negative control group, respectively). Meanwhile, a medium containing 1% phenol was set as a positive control. According to GB/T 16886.1/ISO 10993–1, a material is regarded as non-toxic when the RSR for 100% extract is over 70%. Additionally, the hemocompatibility of the SIS and E-SIS was evaluated with a hemolysis test and SEM.

To evaluate cell adhesion, the NIH-3T3 cells were directly seeded onto the various patches. After 24 h of cultivation, the cells were fixed with neutral formaldehyde. Subsequently, they were permeabilized and stained with phalloidin for cytoskeleton observation, or underwent gradient dehydration with alcohol and CO_2 critical point drying for SEM testing.

2.7. Evaluation of immunomodulatory property

Likewise, the RAW264.7 cells were pre-treated with 100 ng/mL LPS for 6 h prior to culturing with extractions derived from various patches for another 48 h. The polarization of cells was measured with flow cytometry, immunofluorescence staining as well as real-time quantitative PCR (qPCR). Primers are given in Table S1. Meanwhile, the expression of cytokines, including tumor necrosis factor-α (TNF-α), interleukin-6 (IL-6), and inducible nitric oxide synthase (iNOS), was evaluated with enzyme-linked immunosorbent assays (ELISA) by following the manufacturers' protocols.

Furthermore, the overall transcriptional characteristics of the RAW264.7 after aforementioned treatments were analyzed with high-throughput RNA sequencing. The differentially expressed genes (DEGs) were first filtered and submitted to the gene ontology (GO)

function and Kyoto Encyclopedia of Genes and Genomes (KEGG) pathway enrichment analysis.

2.8. Evaluation of anti-oxidative property

1,1-Diphenyl-2-picrylhydrazyl (DPPH) assay was carried out to evaluate free radical scavenging ability of the E-SIS. Briefly, various patches were immersed into 100 μM DPPH with continuous rotation for 30 min. DPPH scavenging rate was calculated with: $DPPH\ Scavenging\ rate\ (\%) = (OD_0 - OD_t) / OD_0 \times 100\%$ (where OD_0 and OD_t respectively denoted the initial and final absorbance at 519 nm). For cellular experiments, the NIH-3T3 cells were cultured with various CM containing 100 nM H_2O_2 for 24 h. Intracellular ROS was measured with a 2, 7-dichlorofluorescein diacetate (DCFH-DA) probe. Meanwhile, other oxidative indicators including lipid peroxidation level and catalase (CAT) activity were also analyzed by following the manufacturer's protocols.

2.9. Evaluation of immunomodulatory effects on the HUVECs and NIH-3T3 cells

Transwell and scratch assays were performed to assess the immunomodulatory effects of various patches on the HUVECs and NIH-3T3 cells. For transwell assay, the cells were seeded in the upper chamber, while the lower chamber was filled with CM from various patches. After 24 h of culture, the cells were fixed and stained with crystal violet for observation. As for the scratch test, when cell confluence has exceeded 90%, medium with 1% FBS was replaced overnight. On the next day, a scratch was made with a 200 μL pipette tip, and the cells were cultured with CM containing 1% FBS for an additional 36 h. The healing rate was calculated as follows: $Healing\ rate\ (\%) = (S_0\text{-}S_m)/S_0 \times 100\%$ (Where S_0 represents the original scratch area; S_m represents the scratch area at the pre-scheduled time point).

qPCR and immunofluorescent staining were performed to assess the immunomodulatory effects of various patches on the collagen synthesis by the NIH-3T3 cells. In short, the NIH-3T3 cells were cultured with CM derived from various patches. The expression of collagen type I alpha 1 chain (*Col1a1*) and collagen type III alpha 1 chain (*Col3a1*) was evaluated with qPCR and primers given in Table S2. In addition, the intracellular protein level of COL1A1 and COL3A1 were also evaluated by immunofluorescent staining.

qPCR, ELISA, and immunofluorescent staining were carried out to assess the immunomodulatory effects of various patches on the angiogenic capacity of the HUVECs. Likewise, the HUVECs were cultured with various CM. The expression of vascular endothelial growth factor (*Vegf*), hypoxia-inducible factor 1(*Hif-1α*), and *Notch* were evaluated by qPCR with primers given in Table S3. Meanwhile, intra- and extra-cellular protein levels of VEGF were measured with immunofluorescent staining and ELISA, respectively. Furthermore, a tube formation assay was performed to assess the angiogenesis with various CM. Details are shown in the Supplementary Materials.

2.10. In vivo animal study

To further evaluate the *in vivo* therapeutic efficacy of the E-SIS, a full-thickness skin defect model on the Sprague Dawley rat (SD rat) was constructed. The study protocol was approved by the Animal Care and Use Committee of Sichuan University (No.20221128006) and has conformed to the principles of laboratory animal care issued by the National Medical Research Association. Briefly, the dorsal of the rats was shaved and thoroughly disinfected after anesthetizing. Thereafter, 10 mm full-thickness wound defects were made symmetrically on both sides of the back and fixed with metal rings to prevent the contraction of dorsal muscles, so that the defects could only be healed by granulation and re-epithelization to mimic the healing process in humans. The SIS or E-SIS patches were simultaneously sutured onto the wound area with the metal rings. Additionally, a macrophage depletion model was implemented for assessing the immunomodulatory effects of the E-SIS on wound healing. Detailed information can be found in the Supplementary Material.

At pre-scheduled time points, the appearance of skin defect was photographed. Thereafter, the SD rats were euthanized for histological analysis. The samples were successively fixed, dehydrated, and embedded in paraffin blocks. Tissue sections with a thickness of 4 μm were prepared from the central area for Hematoxylin and Eosin (H&E) staining, Masson staining, and Sirius Red staining. Meanwhile, immunofluorescence staining was carried out to further evaluate the inflammation, macrophage polarization, and angiogenesis in the regenerative area.

2.11. Statistical analysis

All experiments were performed in at least triplicate. Data were presented by the mean ± standard deviation (SD) and analyzed by one-way analysis of variance (ANOVA) in conjunction with Tukey's multiple comparison tests for pairwise comparison. All analyses were carried out with GraphPad Prism 8.0.2 software. $p < 0.05$ was considered statistically significant.

3. Results and discussion

3.1. Characteristic of the E-SIS

Digital images of various patches were presented in Fig. 2A. After EGCG crosslinking, the color of the SIS underwent a concentration-related transition to brown. Typically, pigmentation may result from the oxidative polymerization of polyphenolics, which can lead to formation of colored compounds such as quinonoids. Besides, the topological structure of the SIS observed by SEM revealed a heterogeneous change on the two sides. The mucosal side of the SIS has naturally displayed a loose structure, with collagen fibers confoundly arranged. Under the strong cross-linking effect of the EGCG, the collagen fibers have become neater and denser, and some have aggregated together, which may be attributed to the formation of hydrogen bonds between the EGCG and the SIS alongside the mutual adhesion amongst the nanofiber bundles [24]. By contrast, the muscular layer of the SIS has exhibited greater smoothness and density, showing no discernible collagen fiber-like structure. Consequently, the EGCG has primarily adhered to the surface, conferring a negligible effect on surface morphology (Fig. S1).

The crosslinking rate was then evaluated with an OPA assay, which could reflect the content of the free amino group on various patches. As shown in Fig. 2B, the crosslinking rate has significantly increased to 40.69 ± 1.57% and 62.09 ± 1.88% when the concentration of EGCG had reached 0.5% and 2%, respectively. Meanwhile, FTIR was used to further elucidate the physicochemical attributes of the E-SIS. Transmittance result has shown a significant decrease at 1645 cm^{-1} and 1544 cm^{-1}, which could be respectively attributed to the C═O and stretching vibrations coupled with N–H bending from amide linkage (Fig. 2C). Although the FTIR spectra of the E-SIS showed no new shifts compared with the SIS spectrum, the O–H and N–H stretching vibration peak at 3306 cm^{-1} has decreased dramatically and even vanished completely.

The hydrophilicity of each patch was subsequently assessed. Fig. 2D and E demonstrated that the Water Contact Angle (WCA) of the SIS was approximately 82.16 ± 3.0°, which has diminished by nearly 20° following the EGCG crosslinking. The marked reduction in WCA has indicated enhanced hydrophilic characteristics of the unprocessed SIS patch. This enhancement could be ascribed to the presence of a considerable number of hydrophilic groups in the phenolic building blocks of the EGCG molecule. Meanwhile, since the surface hydrophily plays a key role in cell proliferation and adhesion, such improvement may foster a more conducive environment to promote cell adhesion

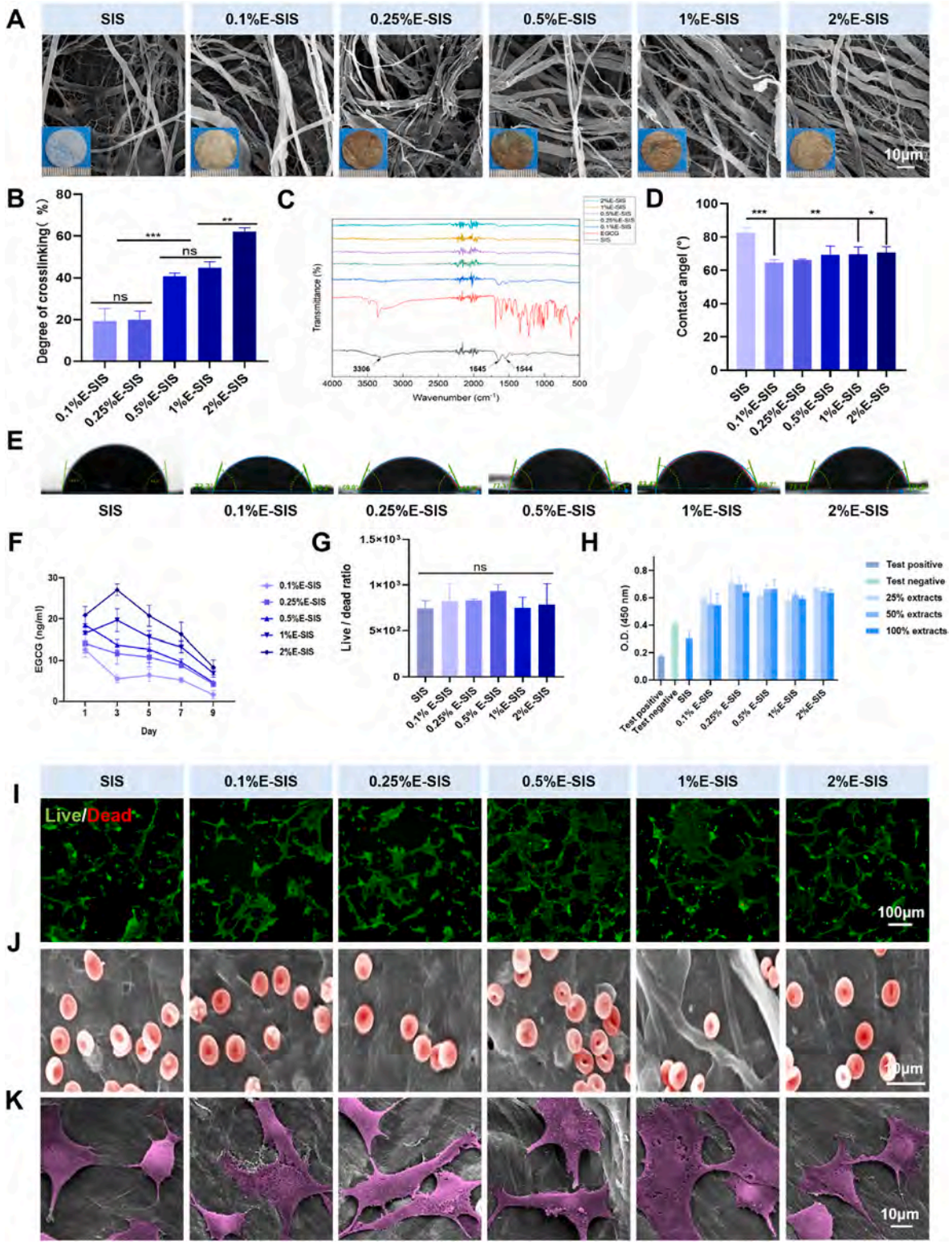

Fig. 2. Characterization and biocompatibility of the E-SIS: (A) Surface morphology of the mucosal side; (B) Degree of crosslinking; (C) FTIR; (D–E) Water contact angles represent photographs and quantitative statistics; (F) Release profile of EGCG; (G&I) Live and dead staining and semi-quantitative analysis; (H) NIH-3T3 cells viability was measured by CCK8; (J) SEM image of red cells; (K) SEM images of NIH3T3 cells. ns: $p \geq 0.05$, $^{*}p < 0.05$, $^{**}p < 0.01$, $^{***}p < 0.001$. (For interpretation of the references to color in this figure legend, the reader is referred to the Web version of this article.)

when implanted *in vivo* [25,26]. The EGCG release profile was also measured. *In vitro* experiments showed that the release of EGCG could last for 9 days or even longer (Fig. 2F). Interestingly, the 0.1%–0.5% E-SIS attained the highest release on the first day, while 1% and 2% E-SIS attained the maximum release on the third day, the release of each group has then decreased with time. These demonstrated that the SIS has successfully crosslinked with the EGCG. The modified SIS patch exhibited a denser microstructure, improved hydrophily, and a

sustained EGCG release. The influence of such alterations on its therapeutic efficacy for wound healing was systematically evaluated in subsequent experiments.

3.2. Evaluation of biocompatibility and cellular adhesion

Good biocompatibility is a prerequisite for the application of wound dressings. Herein, both cytocompatibility and hemocompatibility were

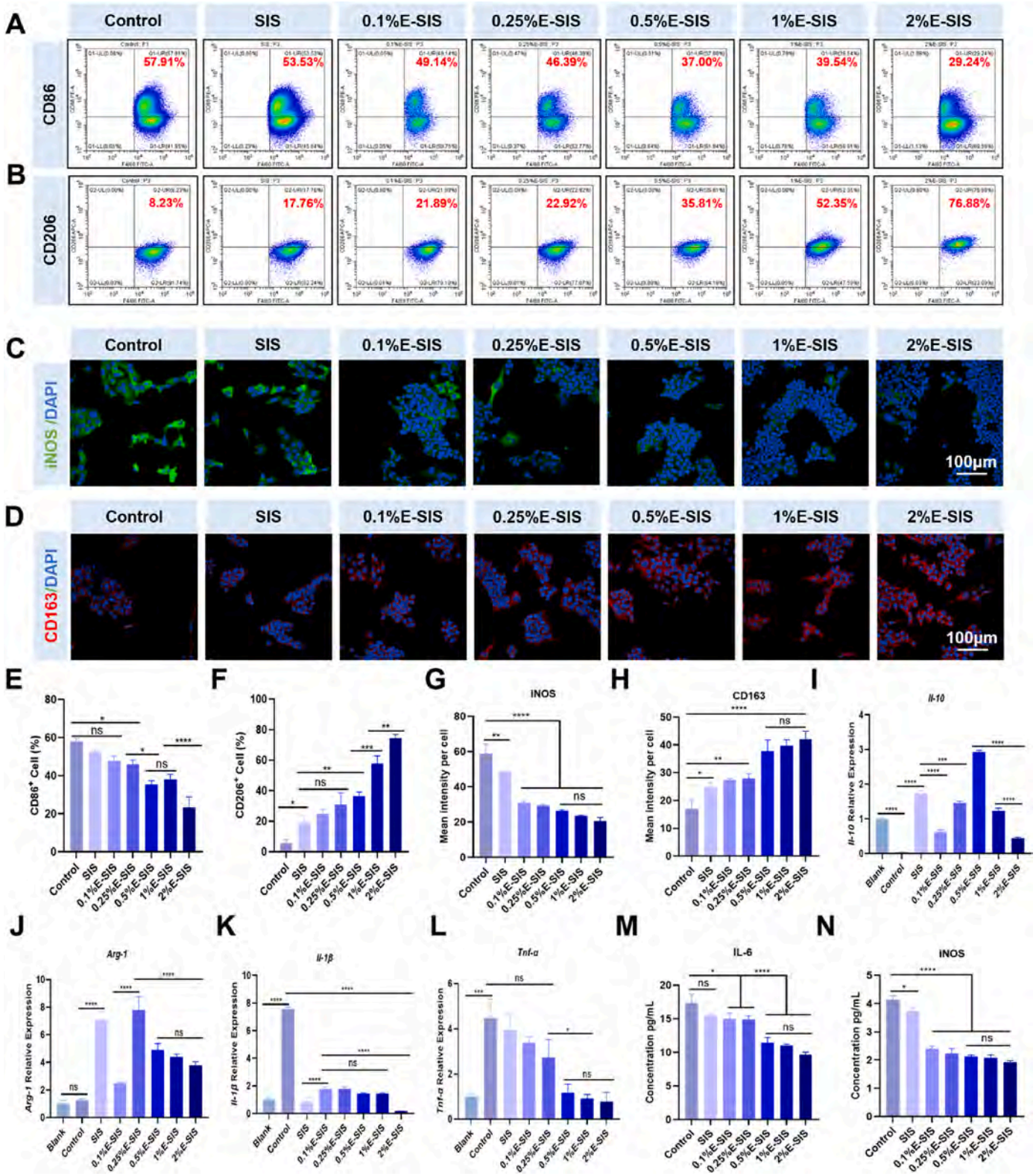

Fig. 3. Evaluation of immunomodulatory effects A&E: Flow cytometry results for CD86 expression. B&F: Flow cytometry results for CD206 expression. C&G: Results of immunofluorescence staining of iNOS. D&H: Results of immunofluorescence staining for CD163. I–L: Expression of *Il-10*, *Arg-1*, *IL-1β*, *Tnf-α*. *M*–N: The levels of IL-6 and iNOS in RAW264.7. ns: $p \geq 0.05$, $^{*}p < 0.05$, $^{**}p < 0.01$, $^{***}p < 0.001$, $^{****}p < 0.0001$.

first assessed *in vitro*. Live/dead staining illustrated that both the NIH-3T3 cells and the HUVECs had sustained a satisfactory survival status on the surface of various E-SIS, with negligible evidence of dead cells (Fig. 2G and I and Fig. S2). Meanwhile, the viability of cells, as measured by a CCK-8 assay, indicated that the RSRs of NIH-3T3 cells, cultured in extracts from the E-SIS at various concentrations, have exceeded 70%. This has complied with the national standards for the biocompatibility requirements of implanted scaffolds (Table S4). Furthermore, we have found that the E-SIS extraction could promote the proliferation of the NIH-3T3 cells (Fig. 2H). Additionally, no rupture of red cells on the surface of the E-SIS was detected by SEM (Fig. 2J), and no significant hemolysis was observed when in contact with the E-SIS (Fig. S3). In fact, the SIS itself is comprised of a large amount of collagen and bioactive molecules, which are inherently nontoxic for cells [27–29]. Besides, the heparin and heparin sulfate on the SIS also endowed it with intrinsic anticoagulant activity as well as blood compatibility [30].

Additionally, cell adhesion was observed by SEM and cytoskeleton staining. As shown in Fig. 2K and S4A, fewer pseudopodia were extended when the NIH-3T3 and RAW264.7 were seeded onto the SIS patch in comparison to various E-SIS patches. Cytoskeleton staining also confirmed an increase in the cell adhesion area on the EGCG-modified SIS patches (Fig. S4B). These indicated that the presence of EGCG did not affect on the fibronectin, laminin, and RGD sequences in the SIS. And the enhancement in hydrophily could further improve cellular adhesion. Moreover, the catechol groups in the EGCG may also interact with the amino and thiol groups on the cytomembrane to promote adhesion [31, 32]. Taken together, the above results demonstrated that the E-SIS has possessed superior biocompatibility and adhesion ability, which are favorite for its use in biomedical applications.

3.3. Evaluation of the immunomodulatory properties of the E-SIS

It has been widely recognized that a favorable immune microenvironment, characterized by timely and proper transition from inflammation to proliferation and remodeling phases as aforementioned, plays a significant role in the process of tissue repair [33–35]. Given the outstanding immunomodulatory effects of the EGCG, we anticipated that its modification could equip the SIS patches with corresponding functions to promote the shift of M1-to-M2 polarization of macrophages.

To verify this, the RAW264.7 were transiently treated with LPS to simulate the inflammatory response prior to the culturing with extractions from various patches [36,37]. Flow cytometry revealed that the LPS treatment could trigger the M1 polarization of the macrophages, as evidenced by the rapidly increasing expression of CD86 (Fig. 3A and E). The CD86-positive cells in the SIS group were slightly reduced to 52.58 $\pm$ 1.94%. When the concentration of the EGCG exceeded 0.25%, the E-SIS started to suppress the CD86 expression, with the 2% E-SIS showing the most potent anti-inflammation capacity (23.39 $\pm$ 5.41%). Accordingly, the percentage of CD206-positive M2 macrophages has increased with the concentration of EGCG. Likewise, the 2% E-SIS showed the highest efficacy to promote the M2 macrophage polarization (74.38 $\pm$ 2.39%) (Fig. 3B and F). Other biomarkers of the M1 and M2 macrophages were further analyzed with immunofluorescence staining. As shown in Fig. 3C and G, the LPS treatment has effectively increased the expression of M1-related iNOS [38]. By contrast, the E-SIS effectively reversed such an increase while up-regulated the M2-related CD163 expression (Fig. 3D and H) [39].

Expression of the gene encoding macrophage-secreted cytokines was subsequently evaluated by qPCR. Along with the M1 polarization induced by the LPS, expression of pro-inflammatory intermediates like *Il-1β* and *Tnf-α* has dramatically increased (Fig. 3K and L). Both the SIS and E-SIS could significantly suppress LPS-triggered up-regulation of inflammatory intermediates (except *Tnf-α* for pristine SIS), while inducing the expression of pro-healing cytokines including *Il-10* and *Arg-1* (Fig3. I and J). Furthermore, as revealed through the ELISA assay, the E-SIS displayed superior regulatory effects on the protein levels of IL-6, iNOS, and TNF-α, compared with the SIS (Fig. 3M and N and Fig. S5).

Inflammation serves a pivotal role in the process of tissue repair. Particularly, a specific extent of inflammation is advantageous for tissue repair, encompassing the eradication of pathogenic microorganisms to the initiation of early recruitment. Studies have confirmed that the depletion of macrophages during the inflammation phase can significantly reduce the formation of vascularized granulation tissue and impair the epithelialization [40]. Nevertheless, any dysfunction of this may significantly impede the repair process [41]. Excessive activation of inflammation may disrupt the function and activity of multiple cells implicated in the tissue repair. Moreover, it may directly trigger the expression of matrix metalloproteinase proteins and serine proteases and damaging of the local extracellular matrix, thereby accentuate the tissue injury [42]. The seemly shift to M2 macrophage-dominated immune microenvironment not only could confine the inflammatory to an appropriate range but may benefit wound healing through various pro-healing growth factors [43,44]. Of note, our study showed that pristine SIS also showed certain immunomodulatory effects, which may be attributed to the intrinsic component of the SIS. Decellularization has allowed the SIS to retain substantial amounts of collagen, glycosaminoglycan, and proteoglycan, as well as a variety of bioactive molecules which may stimulate cell adhesion, proliferation, and differentiation [45]. Such stimulation in turn may influence the immunomodulatory behaviors of the macrophages, thereby affecting their immunomodulatory behaviors [46]. Previous studies have established that decellularized membranes can trigger type 2 immune responses, and macrophages found at the SIS implantation site predominantly exhibited an M2 phenotype [47–50]. However, our study additionally uncovered that the immunomodulatory impacts of pristine SIS were deficient, implying the necessity for further modifications. The above results suggested that the EGCG modification could dramatically enhance the immunomodulatory effects of the SIS patches to promote the M1-to-M2 transition of the macrophages, along with regulation of the expression of relevant cytokines, thereby providing a favorable immune environment for wound healing. In consideration of the equivalent immunomodulatory effects demonstrated by the 0.5%–2% E-SIS, we have selected 0.5% E-SIS for the subsequent experiments.

3.4. Transcriptome analysis

To further elucidate the mechanism underlying the immunomodulatory effects of the E-SIS, RNA-seq was carried out to evaluate the transcriptional profiles of the RAW264.7 cultured with various extractions. Principal component analysis has suggested benign intragroup homogeneity (Fig. 4A). Meanwhile, we have identified 931 differentially expressed genes (DEGs) (378 up-regulated and 553 down-regulated) between the SIS and control groups, as well as 972 DEGs (including 341 up-regulated and 631 down-regulated) between the E-SIS and control groups (Fig. 4B and C). Intriguingly, most DEGs were found between the SIS and E-SIS groups (including 900 up-regulated and 1223 down-regulated), indicating that the EGCG in the E-SIS was the major factor driving the differential gene expression (Fig. 4D).

Heat map indicated an up-regulation of chemokine-related genes in the E-SIS group such as Chemokine CC-Ligand 2 (*Ccl-2*), Chemokine CC-Ligand 7 (*Ccl-7*), and Chemokine CXC Ligand 10 (*Cxcl-10)* (Fig. 4E). A further functional enrichment analysis was conducted using the GO and KEGG databases. Several signal axes related to immune response including TNF signaling pathway, JAK-STAT pathway and Toll-like receptor signaling pathway *etc*. were all regulated by the EGCG (Fig. 4F and G). By such means, the EGCG may exert its immunomodulatory effects. In conclusion, the E-SIS has the potential in mitigating local inflammation during the inflammatory stage, thus fostering an improved environment for tissue repair and regeneration. Therefore, we have subsequently examined how such immunomodulatory effects on the macrophages may influence the healing process in subsequent experiments [19].

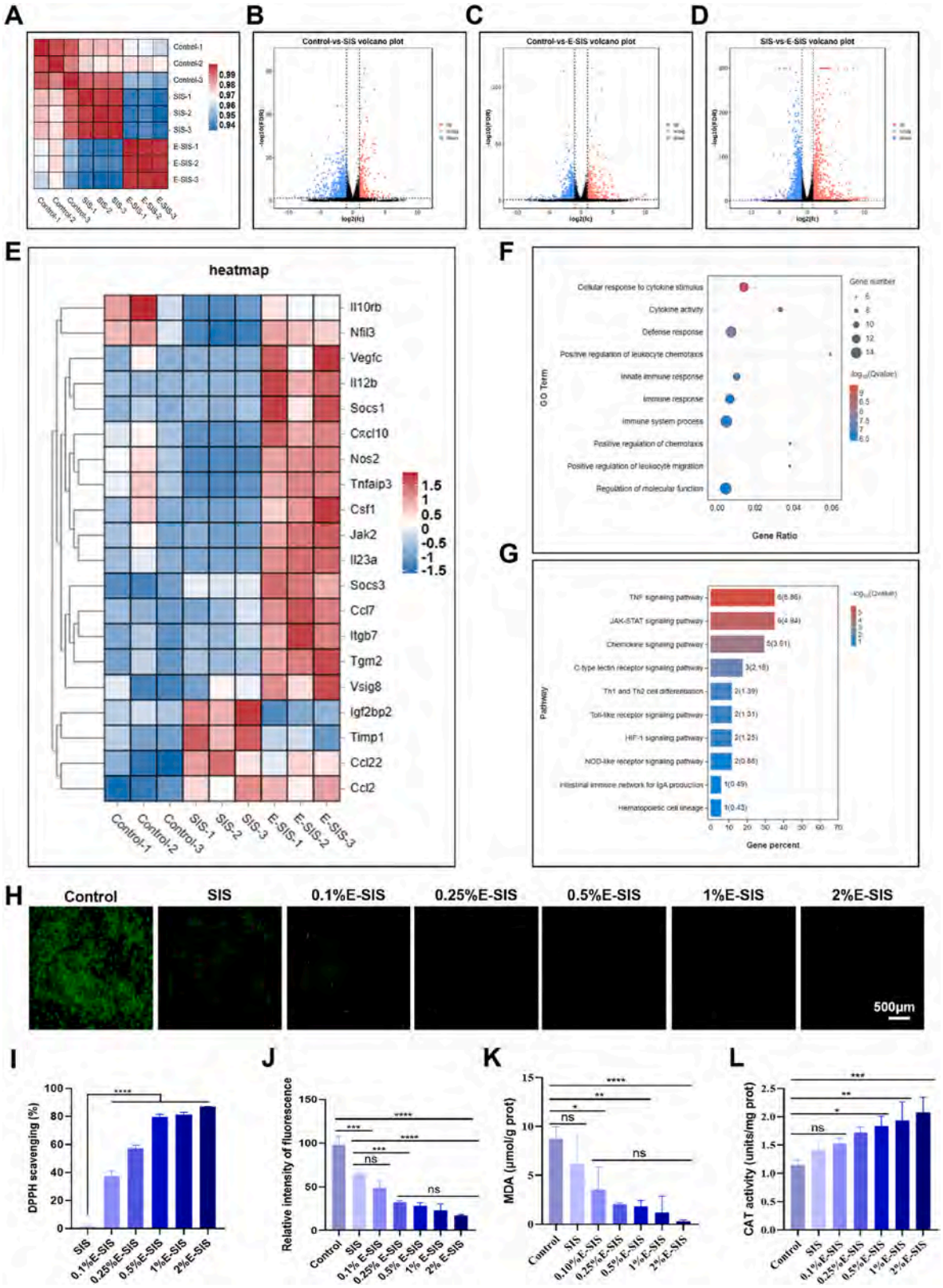

Fig. 4. Correlation of gene expression among various samples and analysis of differential gene expression and antioxidant capacity of the NIH-3T3 treated with various CM: (A) Principal component analysis; (B–D) Differential gene analysis between the groups. (E) Heat map of DEGs. (F) GO analysis. (G) KEGG analysis. (H&J) Intracellular ROS content. (I) DPPH scavenging ratio. (K) Intracellular MDA content. (L) Intracellular CAT activity. ns: $p \geq 0.05$, *p < 0.05, **p < 0.01, ***p < 0.001, ****p < 0.0001.

3.5. Evaluation of the antioxidant properties of the E-SIS

At the initial stage of inflammation, the localized enrichment of ROS has exhibited substantial bactericidal effects. However, the resultant oxidative stress could inadvertently lead to tissue damage and impede tissue repair [51–53]. As a naturally occurring polyphenol, the abundant phenolic hydroxyl groups can endow the EGCG with outstanding free radical scavenging ability [54].

To confirm whether the E-SIS possess the specific properties of the EGCG, we have evaluated their antioxidative capacity. As shown in Fig. 4I, the DPPH assay showed that the E-SIS has displayed robust free radical scavenging ability. When the concentration of EGCG exceeded 0.5%, the clearance rate surpassed 75% and further increased to 86.83 ± 0.39% for 2% E-SIS. To further validate the anti-oxidative stress ability *in vitro*, the NIH-3T3 cells were cultured with CM containing H_2O_2 for simulating the local environment. As demonstrated by a DCFH-DA probe, intracellular ROS has significantly accumulated in the control group (Fig. 4H and J). Whereas when the concentration of the EGCG reached 0.25%, the E-SIS has successfully relieved the oxidative stress of the NIH-3T3 cells and emitted weak fluorescence, with 2% E-SIS

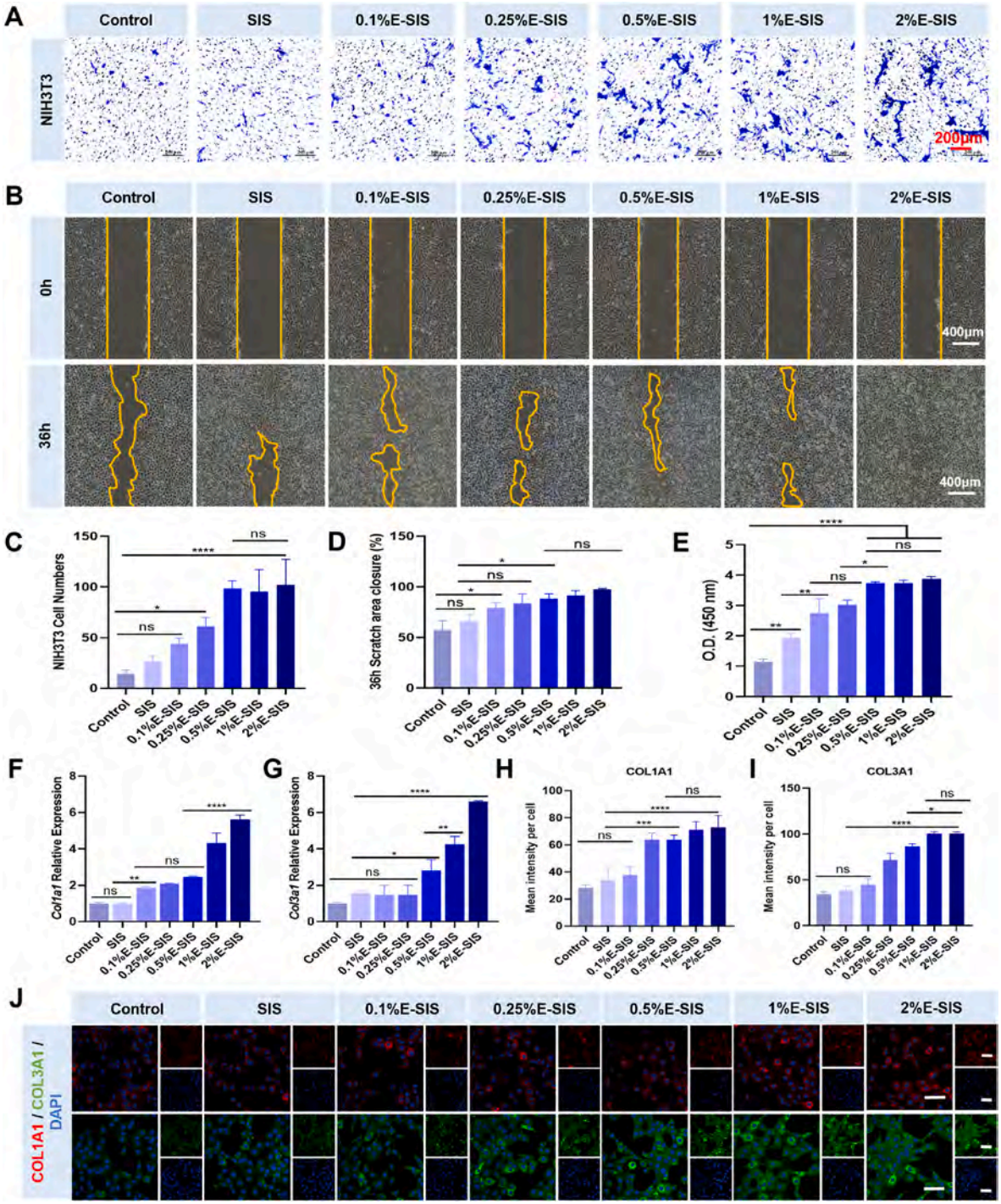

Fig. 5. Effect of immunomodulation on NIH3T3 cells A–D: Images of cell migration and quantitative analysis; E: Proliferation of NIH-3T3 cells; F–G: Gene expressions of *Col1a1* and *Col3a1*; H–J: Immunofluorescence expression and quantification of COL1A1 and COL3A1. Scale bar = 100 μm. ns: $p \geq 0.05$, *$p < 0.05$, **$p < 0.01$, ***$p < 0.001$, ****$p < 0.0001$.

showing the best ROS scavenging ability yet with no significant difference with 0.25% E-SIS. The level of lipid peroxidation, as measured by MDA, also showed a dramatic increase after H_2O_2 treatment while maintaining a relatively low level in each E-SIS group (Fig. 4K). In addition, CAT activity was also evaluated. Compared with the control group, the enzyme activity of CAT showed no difference between the SIS and 0.1% E-SIS groups. Nevertheless, when the concentration of EGCG reached 0.25%, CAT activity within the E-SIS group has markedly increased, indicating that an E-SIS concentration exceeding 0.25% could prevent oxidative stress damage (Fig. 4L).

As a small molecule, the ROS is easy to diffuse into the tissue environment. It is worthy noting that, in addition to the direct damage to normal tissues, the ROS is also a key participant to the inflammatory response and plays an important role in various signal transductions [55]. Untimely intervention of the oxidative stress will inevitably lead to persistent inflammation and bring great obstacles to the wound repair [56]. Even though pristine SIS had exhibited some DPPH scavenging ability, which may be attributed to certain anti-oxidative peptides and/or polysaccharides, such effect could reduce the MDA level and/or up-regulate the CAT activity after H_2O_2 treatment which, as demonstrated by previous studies, may play significant roles in wound healing [57–59]. Our results suggested that the EGCG modification could dramatically enhance the free radical scavenging property and protect the cells from oxidative stress. Meanwhile, the E-SIS can also activate the endogenous antioxidant system to further counteract the detrimental effect of local ROS. In further experiments, we have explored how the improvement in both immune and oxidative microenvironments could influence the behavior of the NIH-3T3 cells and HUVECs *in vitro*.

3.6. Effects of immune microenvironment on the NIH-3T3 cells

Fibroblasts are the most dominate cellular component of skin tissue and responsible for the production and remodeling of ECM. A substantial body of evidence has elucidated the complex and dynamic relationship between the fibroblasts and immune microenvironment [60]. In short, the macrophages can modulate the behavior of fibroblasts by secreting cytokines like TGF-β, which in turn may stimulate the proliferation of fibroblasts and ECM production. Furthermore, the macrophages not only can phagocytize apoptotic fibroblasts but also maintain the balance between the ECM production and degradation [61]. Given the intricate interactions between the macrophages and fibroblasts, we have assessed how the improvement of immune microenvironment may affect the migration, proliferation, and collagen deposition of the NIH-3T3 cells.

As evidenced by the transwell assay, the inflammatory microenvironment was not conducive to cell migration. Only a mean of 14 ± 4 cells has crossed the membrane (Fig. 5A and C). By contrast, the number of migrated NIH-3T3 cells in the 0.5%–2% E-SIS have shown a nearly ten-fold increase. Similarly, the scratch assay revealed that the healing rates in both the control and the SIS groups were less than 70%, but had surged to approximately 85% in various E-SIS groups (Fig. 5B and D).

Another significant factor influencing the tissue repair is collagen synthesis. Collagens surrounding nascent cells can stimulate the formation of new blood vessels and epithelial coverage, thereby fostering wound healing [62]. Hence, we have analyzed the impact of the immune microenvironment shaped by various patches on the production of collagens. On one hand, the escalation of collagen types I and III has hinged on the number of fibroblasts [62]. The proliferation assay indicated that, compared with the control group, the cell count in the SIS group only registered a slight increase. However, when the concentration of EGCG had exceeded 0.5%, a significant cell count increment was observed (Fig. 5E). On the other hand, alongside the expected increase in cell numbers, qPCR results also showed that, compared with the control group, expression of the *Col1a1* gene in the NIH-3T3 cells did not increase in the SIS group. By contrast, with the 0.1%–2% E-SIS, there was a significant increase by 1.9–5.6 times (Fig. 5F). Similarly, the expression of *Col3a1* gene also showed a similar trend (Fig. 5G).

To confirm the collagen expression at the protein level, immunofluorescence staining was carried out. As shown in Fig. 5H-J, there was a notable up-regulation of the fluorescence signals in both COL1A1 and COL3A1 within the 0.25%–2% E-SIS groups. Likewise, the immune microenvironment moderated by the SIS group appeared to influence the fibroblasts through its inherent bioactive factors. Nevertheless, it is important to note that these results had little or no statistical significance, suggesting that the SIS has not contributed positively to the wound repair in an inflammatory environment. By contrast, our results demonstrated that the immune microenvironment regulated by the E-SIS group showed a beneficial effect by positively influencing the migration, proliferation, and collagen deposition of the fibroblasts, thereby promoting the skin repair effectively.

3.7. Effects of the immune microenvironment on the HUVECs

Apart from fibroblasts, vascular endothelial cells also play a critical role in wound healing, particularly through their participation in angiogenesis from the initial skin injury through to the final phase of tissue remodeling [63,64]. During the stage of tissue repair, new capillaries emerged within the wound bed together with the granulation tissue, initiating the establishment of a temporary matrix [65]. A profusion of these new capillaries had quickly proliferated in the wound bed, forming an extensive capillary network that provided essential nutrients and oxygen to the cells within the wound [65].

Likewise, factors produced by the macrophages have also exerted a great influence on angiogenesis [66]. Herein, the CM derived from various patches was utilized to assess the effect of the E-SIS on angiogenesis through immunomodulation. The transwell assay has demonstrated that the HUVECs had migrated more effectively in the E-SIS compared with the SIS, reaching nearly 400 cells when the E-SIS concentration was 0.5% (Fig. 6A and C). Similarly, by the scratch assay, the 0.5% E-SIS exhibited nearly 100% of mobility after 36 h, surpassing the control, the SIS, and other E-SIS groups (Fig. 6B and D). Moreover, the effect of the E–SIS–induced immune microenvironment on angiogenesis was determined from the transcriptional level. qPCR suggested a predominant up-regulation of *Vegf*, *Notch,* and *Hif-1α* gene expression primarily in the 0.5% E-SIS group (Fig. 6E-G). The protein expression of the VEGF mirrored such findings, with 0.5% E-SIS demonstrating the strongest induction effects, as revealed by ELISA and immunofluorescent staining (Fig. 6H-I and K). Furthermore, as revealed by the tube formation assay (Fig. 6J and L), in comparison to the control group, the CM derived from the SIS had exhibited superior angiogenic properties, which may be attributed to the retention of bioactive components such as VEGF, bFGF, and EGF among others [67]. However, the presence of the EGCG had assisted the improvement of the immune microenvironment, thereby further enhancing angiogenesis. Of note, the angiogenesis had paramount when the concentration of the EGCG reached 0.5%, and a further increase in the concentration had led to a decrease in the expression of angiogenesis-related genes.

Existing research has elucidated that the EGCG could deter tumor angiogenesis and metastasis through a dose-dependent reduction of VEGF receptor expression without affecting cell viability [62,63]. Furthermore, the EGCG can curtail angiogenesis via multiple mechanisms such as miRNA, suppression of angiogenic factors, inhibition of receptor phosphorylation, and prevention of VEGF binding with its receptors [64]. Taken together, these suggested that the SIS patches modified with a certain amount of EGCG could foster a beneficial immune microenvironment for angiogenesis.

3.8. Evaluation of in vivo efficacy

Through *in vitro* experiments, we have confirmed that the E-SIS possessed satisfying biocompatibility and immunomodulatory effects to facilitate the M1-to-M2 transition of the macrophages. Given that the 0.5% E-SIS has exhibited the best angiogenic effects, whilst, for the other

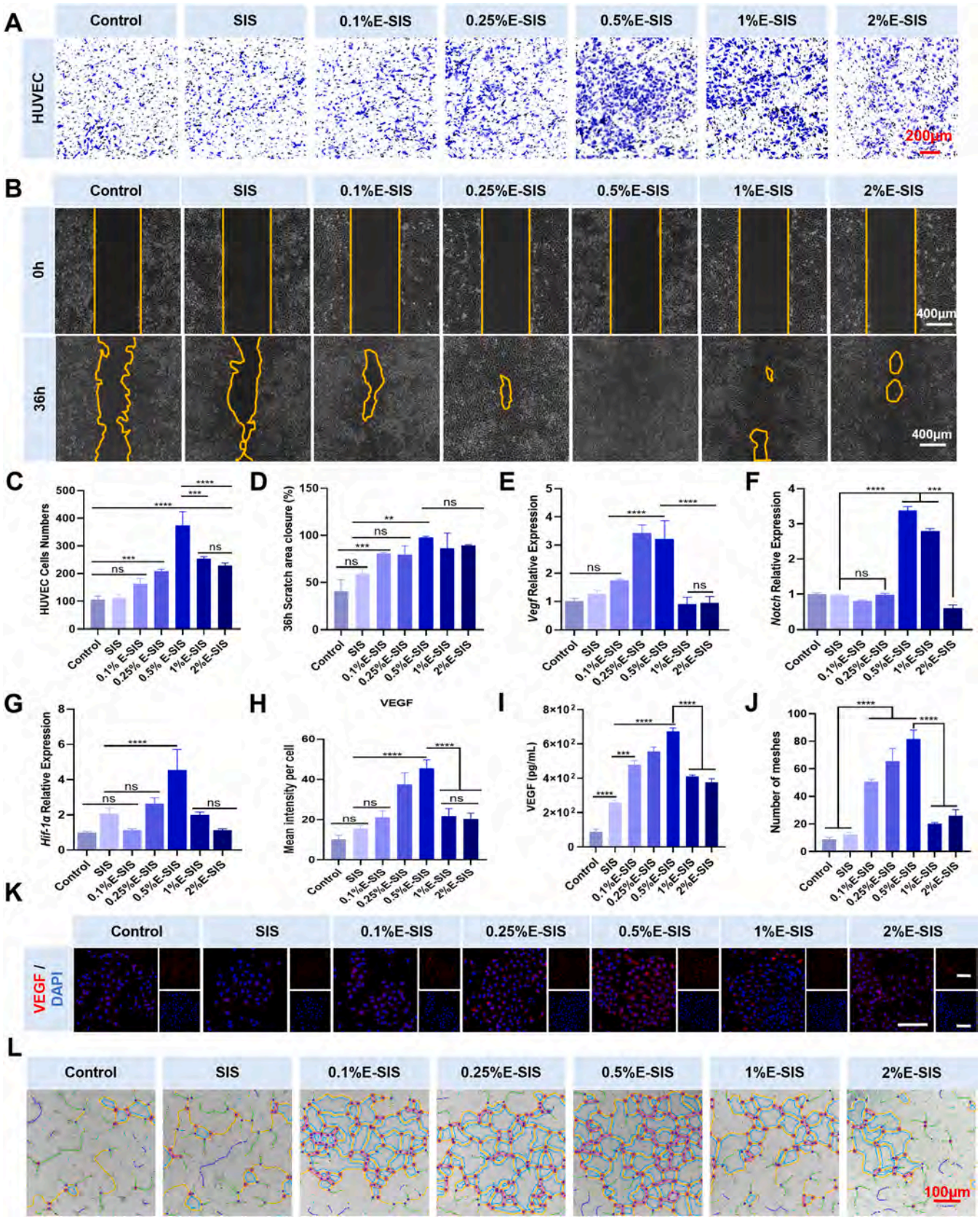

Fig. 6. Effect of immunomodulation on the HUVECs: (A–D) Images of cell migration and quantitative analysis; (E–G) Gene expression of *Vegf*, *Notch* and *Hif-1α*; (H&K) Immunofluorescence expression and quantification of VEGF, Scale bar: 400 μm; (I) The levels of VEGF in the HUVECs. (J&L) Images of tube formation and quantitative analysis. ns: $p \geq 0.05$, *$p < 0.05$, **$p < 0.01$, ***$p < 0.001$, ****$p < 0.0001$.

perspectives 0.5–2% E-SIS demonstrated equivalent impacts, 0.5% E-SIS was selected for the evaluation of *in vivo* efficacy within a full-thickness skin defect model of SD rats and treated with the SIS and E-SIS patches. Those with no additional treatment were set as the control. Meanwhile, to ascertain the role of macrophages in wound healing, especially from the aspect of collagen deposition and angiogenesis, and the immunomodulatory effect of the E-SIS patches on these phenomena, a macrophage-depletion model was also constructed with liposomal clodronate for each treatment (marked as the D-control, D-SIS and D-E-SIS groups, respectively). The injection process is shown in Fig. 7A. The findings from both the immunofluorescence staining of the spleen and flow cytometry of peripheral blood samples suggested that over 70% of

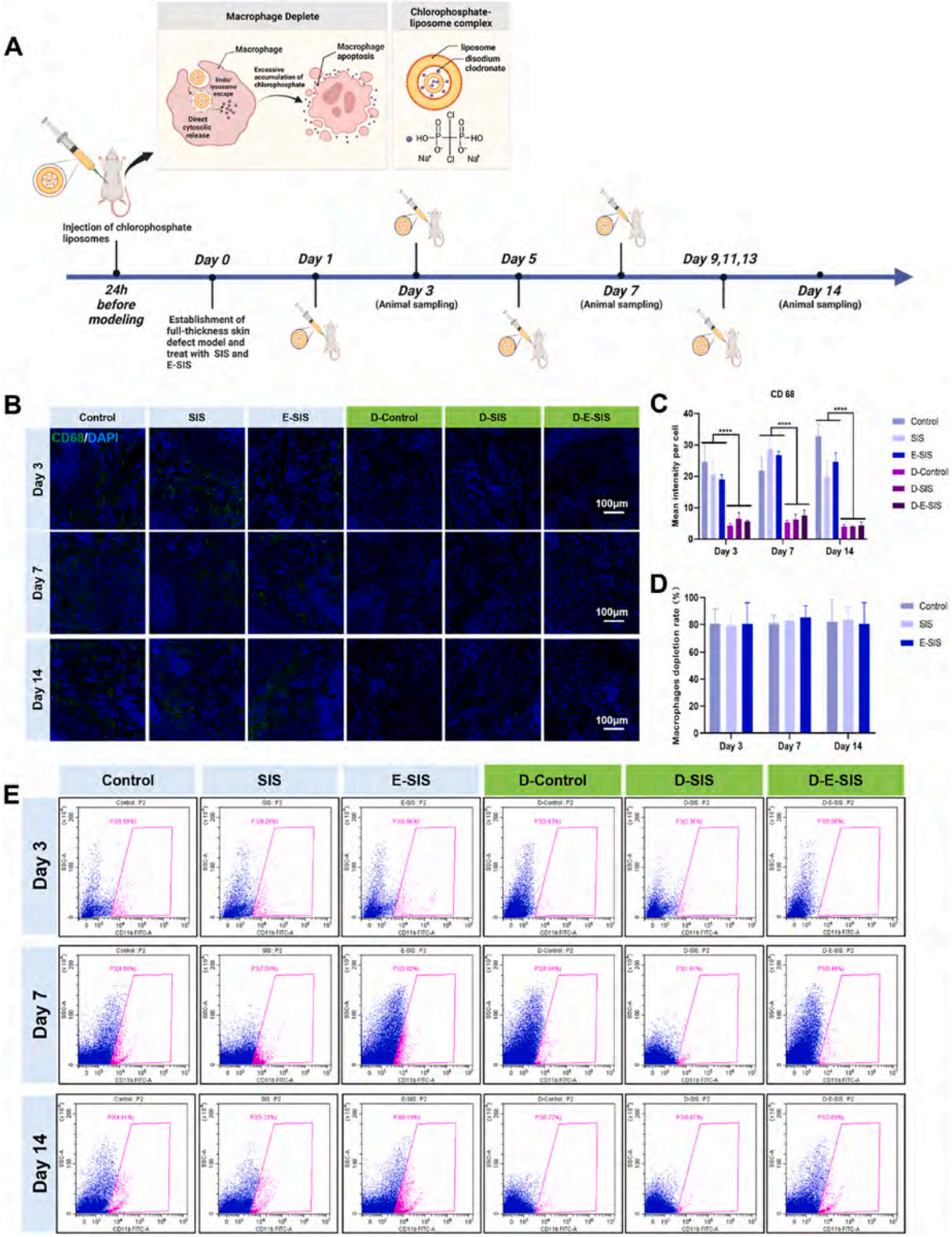

Fig. 7. Establishment of macrophage depletion in SD rats: (A) Schematic overview of macrophage depletion model establishment; (B–C) Immunofluorescence expression and quantitative analysis of CD68 in the spleen of SD rats; (D-E) FC results of SD rat blood CD11b expression and macrophage clearance statistics. , ****$p < 0.0001$

pan-macrophages (indicated by CD68 and CD11b markers) were depleted. This has indicated the successful establishment of the macrophage depletion model (Fig. 7B–E). Meanwhile, H&E staining of vital organs from each group did not reveal any noticeable pathological changes, indicating a favorable *in vivo* safety profile of both the patches and liposomal clodronate (Fig. S7).

The digital images and trajectory map of the wound at each time point are shown in Fig. 8A and C. Although there was no significant difference in the healing rate among the groups on day 3, the defect rate of the E-SIS group was nearly 30%, while it remained over 50% for the other groups by the 7th day (Fig. S8). By day 14, the E-SIS group had continued to show superior repairability. Notably, the group without macrophage depletion had presented a lower defect rate compared with the group with depletion at this point, underscoring the pivotal role of the macrophages in the repairing process. To enhance the precision of our experimental data analysis, we have adjusted the total defect rate for all groups at each time point to one and normalized the data of each group by this total. Likewise, the E-SIS group showed a superior healing rate compared with the control and the SIS groups (Fig. 8B).

A histological evaluation was carried out to further clarify the healing process. By day 3, H&E staining had shown that inflammatory cells were present in all groups. Despite the presence of such cells in the macrophage-depleted group, this suggested that other inflammatory cells are also involved in the skin repair process (Fig. 8D). By day 7, there was minimal epithelial regeneration observed in the E-SIS patch group. Re-epithelialization was evident in all groups until 14 days. Remarkably, the epithelialization of the patches in the E-SIS group has exhibited lower levels compared to both the control and SIS groups (Fig. S9). We have postulated that, during the wound healing process, the thickness of the epithelium will gradually increase and then decrease, whilst the other groups were still at the stage of epidermal thickening. Seven days post-surgery, granulation tissue was identified in all groups. The wound site of the normal SD rats exhibited more granulation tissue as compared with the macrophage depletion group. Among all, the E-SIS group had the thickest granulation tissue, measuring over 2000 μm (Fig. 8E). By 14 days after the surgery, the regeneration of accessory organs was observed under high power fields. The count had exceeded 15 in the E-SIS group and was approximately 10 in the SIS group, and fewer than 5 in the control group. Nevertheless, the regrowth of accessory organs was hardly perceptible across all macrophage depletion groups (Fig. 8F). And only minimal epidermal presence was detected in the depletion groups, whereas normal rats only demonstrated regenerated dermis.

Local inflammation was assessed through immunofluorescent staining. As shown in Fig. 8G and H, the expression of IL-6 was greater in normal rats compared with the macrophage-depleted groups, with the exception of the E-SIS group on both 3 and 7 days post-repair. Additionally, it was observed that the IL-6 expression was highest in the control group, which was followed by the SIS group. The E-SIS group registered a lower IL-6 expression, implying that the E-SIS has played a significant role in anti-inflammatory capacity. By contrast, the expression of CD163 was lower in macrophage-depleted rats compared with normal rats. On day 3, the SIS and E-SIS groups exhibited higher CD163 expression than the control group, with no discernible difference between the SIS and E-SIS groups. This suggested that the SIS has a certain influence on the polarization of macrophages to the M2 type. However, on day 7, the E-SIS group demonstrated the highest CD163 expression, surpassing that of the SIS and control groups (Fig. 9A and B). Above findings suggested that the E-SIS can effectively promote the phenotypic transition of the macrophages and foster a favorable immune microenvironment.

To assess the impact of the immune microenvironment created by the E-SIS on wound healing, we have conducted further studies to measure the collagen synthesis in each group. Masson staining suggested that, on day 7, collagen deposition was scarce among all groups, with the normal rat group outpacing the macrophage depletion group (Fig. 9C and D). Among the normal rats, those in the E-SIS group have shown superior collagen deposition compared with the other groups. By day 14, both the normal and macrophage-depleted rats exhibited increased collagen deposition. Again, the normal rat group showed more collagen deposition than the macrophage depletion group, with the E-SIS group emerging as the most dominant. Furthermore, Sirius red staining was employed to identify the collagen components (Fig. 9E and F). On days 7 and 14, no significant difference was found in the ratio of COL III/COL I between the control and SIS groups. However, a significant difference was observed with the E-SIS group, which displayed a higher ratio of COL III expression compared with the other groups. Conversely, all groups of macrophage-depleted rats showed a lower COL III expression. With regard to angiogenesis, CD31 staining immunofluorescence indicated a higher count of neovascularization in normal rats compared with the macrophage-depleted group on days 7 and 14 (Fig. 9G and H). Furthermore, the E-SIS group had consistently shown optimal angiogenesis at each time point. Simultaneously, a gradual increase in lumen size was observed in normal rats. This has contrasted with macrophage-depleted group which has shown no significant vessel enlargement.

Collectively, in the present study, a novel E-SIS patch was fabricated to improve its therapeutic efficacy as a wound dressing for the treatment of skin wounds. The modified E-SIS patch not only preserved original features such as biocompatibility, bacterial barrier, moisture retention, and bioactivities, but also presented ease of application and provided a reduction in secondary damage caused by recurring dressing changes. Remarkably, the introduction of the EGCG has conferred the patch with antioxidant and immunoregulatory capabilities. Moreover, by improving the microenvironment, the patch has expedited collagen deposition and angiogenesis, thus accelerated the restoration of the skin. Nevertheless, this study also has some limitations. Firstly, the color of the E-SIS has become deeper after modification, which has impeded real-time observation of wound healing. Secondly, the poor water absorption of the E-SIS was not conducive to the healing of wounds with high exudate. Additionally, treatment of special wounds with the E-SIS membrane may demand specific techniques to ensure adequate adhesion and coverage, which may present a challenge for healthcare providers who are unfamiliar with its usage. Finally, although we indirectly reflected the antioxidant capacity of E-SIS through immunological indicators *in vivo* experiments, local oxidative stress levels were not tested.

4. Conclusion

The application of SIS benefits from its high inducible biological activity and mechanical support. Nevertheless, the use of an SIS has been restricted due to its inadequate immunomodulatory properties. To overcome this, we have incorporated EGCG into the SIS. The E-SIS not only exhibited improved hydrophily for effective cell adhesion but also governed a sustained release of EGCG. *In vitro,* experiments further revealed that E-SIS can suppress the inflammatory response and promote the transition of macrophages from M1 to M2 types. Moreover, the E-SIS exhibited remarkable anti-oxidative stress capability, which alleviates oxidative stress damage. Through the enhancement of the local microenvironment, the E-SIS significantly promotes proliferation, migration, and collagen synthesis as well as angiogenesis during tissue repair. The critical roles of an E–SIS–induced immune microenvironment in tissue repair and regeneration were further validated through *in vivo* experiments. Depletion of macrophages notably affected the tissue repair process, diminished the therapeutic efficacy of the E-SIS, and impeded skin regeneration. In conclusion, through this study, we have presented a simple yet effective method to equip the SIS with immunomodulatory capabilities, thereby expanding its applications in wound care.

Declaration of competing interest

The authors declare that they have no known competing financial interests or personal relationships that could have appeared to influence

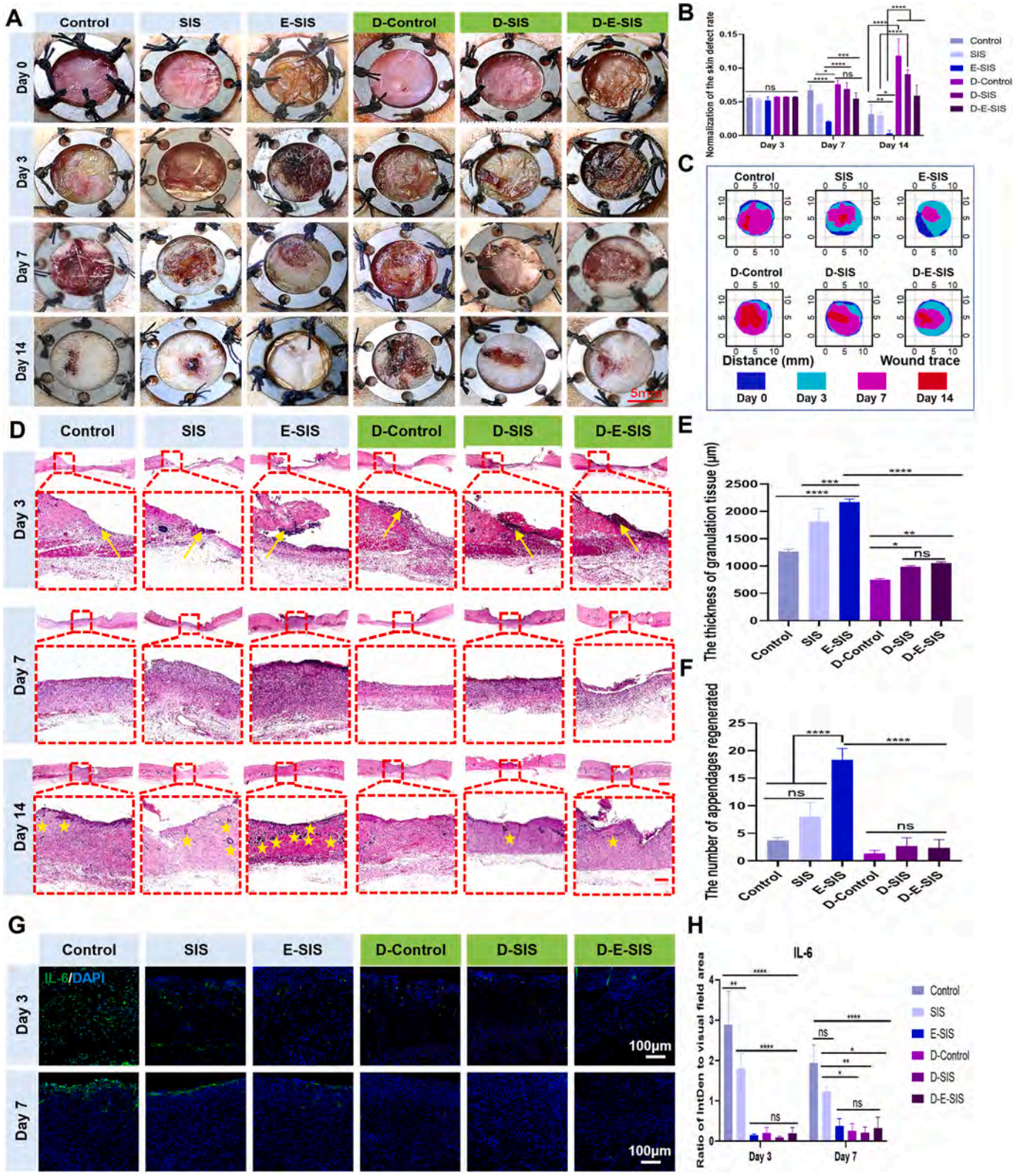

Fig. 8. Evaluation of the therapeutic effect of the E-SIS *in vivo*: (A–C) Wound healing and quantitative analysis; (D) HE staining and (E) thickness of granulation tissue and (F) Regeneration of appendages, yellow arrow indicated inflammatory cells and yellow star indicated appendages, Scale bar = 1 mm (upper panel) and 400 μm (lower panel); (G) Results of immunofluorescence staining and (H) quantitative analysis of IL-6 around the wound. ns: $p \geq 0.05$, *$p < 0.05$, **$p < 0.01$, ***$p < 0.001$, ****$p < 0.0001$. (For interpretation of the references to color in this figure legend, the reader is referred to the Web version of this article.)

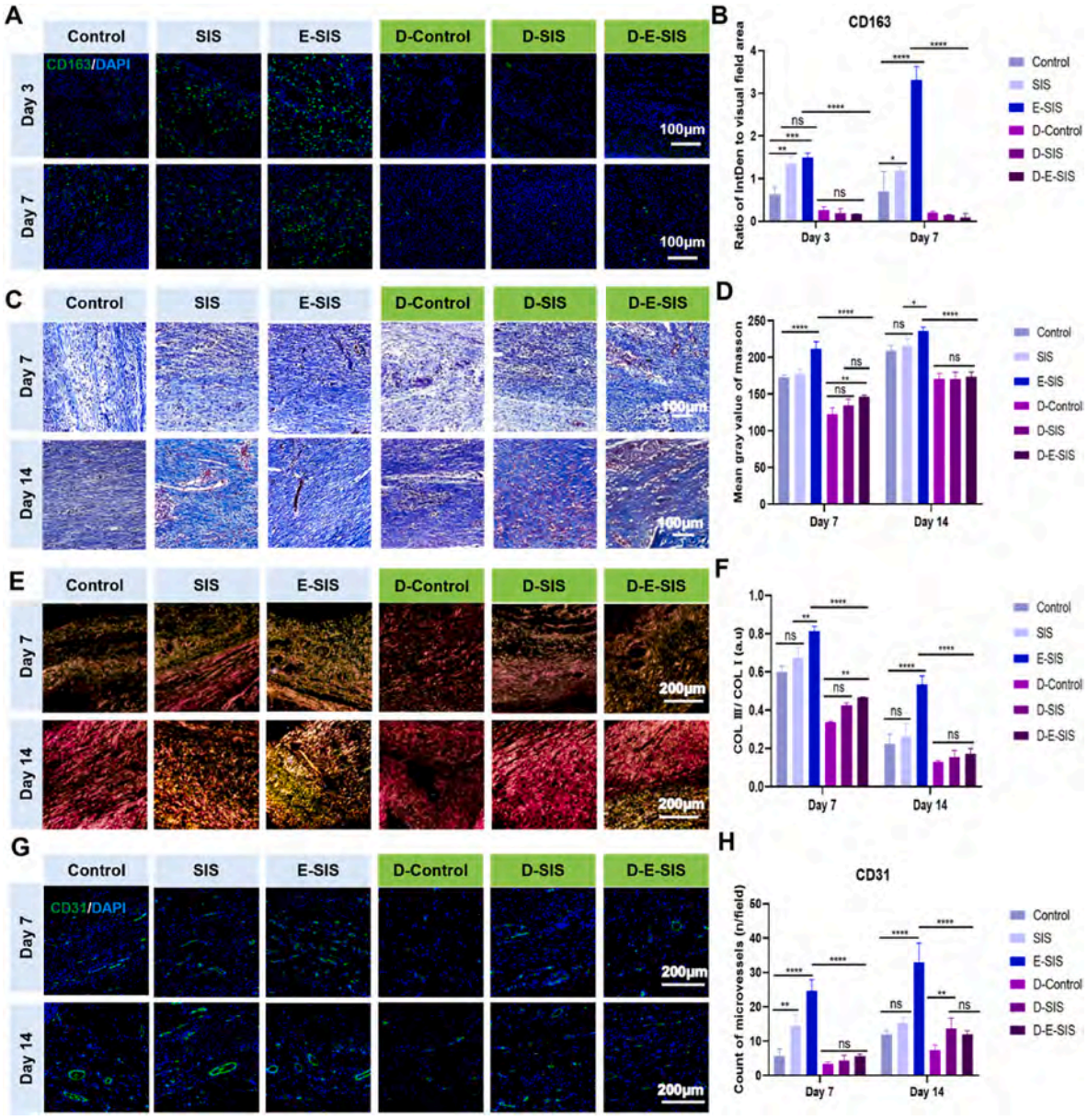

Fig. 9. Evaluation of the therapeutic effect of the E-SIS *in vivo*: (A) Results of immunofluorescence staining and (B) quantitative analysis of CD163 around the wound; (C) Results of Masson staining and (D) quantitative analysis; (E) Results of Sirius red and (F) quantitative analysis; (G–H) Number and quantification of CD31 during the wound healing. ns: $p \geq 0.05$, *$p < 0.05$, **$p < 0.01$, ***$p < 0.001$, ****$p < 0.0001$. (For interpretation of the references to color in this figure legend, the reader is referred to the Web version of this article.)

the work reported in this paper.

Data availability

Data will be made available on request.

Acknowledgement

This study has been jointly supported by the National Natural Science Foundation of China (Grant No. 32171351), the "1.3.5" Project for Disciplines of Excellence, West China Hospital, Sichuan University (Grant No. ZYJC18002), the Frontiers Medical Center, Tianfu Jincheng Laboratory Foundation (TFJC2023010002), and Key Research and Development Program of Sichuan Provincial Department of Science and Technology (Grant No. 2022YFS0097). We gratefully acknowledge for the technical assistance of Histology and Imaging Platform, Core Facility of West China Hospital. Especially, we sincerely thank Ya-Ping Wu for confocal imaging, Bo Su for SEM, Yi Zhang and Wan-Li Zhang and Yue Li for histology analysis.

Appendix A. Supplementary data

Supplementary data to this article can be found online at https://doi.org/10.1016/j.compositesb.2023.111005.

Abbreviations

SIS	Small intestinal submucosa
EGCG	Epigallocatechin gallate
ECM	Extracellular matrix
ROS	Reactive oxygen species
LPS	Lipopolysaccharide

CCK-8	Cell counting kit-8
SDS	Sodium dodecyl sulfate
OPA	O-Phthalaldehyde
WCA	Water contact angle
HUVECs	Human umbilical vein endothelial cells
DMEM	Dulbecco's Modified Eagle Medium
F-12	Nutrient Mixture F-12
FBS	Fetal bovine serum
CM	Conditioned medium
qPCR	Real-time quantitative PCR
ELISA	Enzyme linked immunosorbent assay
DPPH	1,1-Diphenyl-2-picrylhydrazyl
CAT	Cathepsin
MDA	Malondialdehyde
DCFH-DA	2,7-dichlorofluorescein diacetate
CAT	Catalase
Col1a1	Collagen type I alpha 1 chain
Col3a1	Collagen type III alpha 1 chain
Vegf	Vascular endothelial growth factor
Hif-1α	Hypoxia-inducible factor 1α
H&E	Hematoxylin and Eosin
PBS	Phosphate buffer saline
Il-10	Interlekuin-10
Arg-1	Arginase-1
Il-1β	Interlekuin-1β
Il-6	Interlekuin-6
iNOS	Inducible nitric oxide synthase
Tnf-α	Tumor necrosis factor-α
ANOVA	Analysis of variance

References

[1] Xu R, Luo G, Xia H, He W, Zhao J, Liu B, et al. Novel bilayer wound dressing composed of silicone rubber with particular micropores enhanced wound re-epithelialization and contraction. Biomaterials 2015;40:1–11.

[2] Liu W, Gao R, Yang C, Feng Z, Ou-Yang W, Pan X, et al. ECM-mimetic immunomodulatory hydrogel for methicillin-resistant Staphylococcus aureus-infected chronic skin wound healing. Sci Adv 2022;8(27):eabn7006.

[3] Fife CE, Carter MJ. Wound care outcomes and associated cost among patients treated in US outpatient wound centers: data from the US wound registry. Wounds 2012;24(1):10–7.

[4] Rodrigues M, Kosaric N, Bonham CA, Gurtner GC. Wound healing: a cellular perspective. Physiol Rev 2019;99(1):665–706.

[5] Wen Q, Mithieux SM, Weiss AS. Elastin biomaterials in dermal repair. Trends Biotechnol 2020;38(3):280–91.

[6] Hesketh M, Sahin KB, West ZE, Murray RZ. Macrophage phenotypes regulate scar formation and chronic wound healing. Int J Mol Sci 2017;18(7).

[7] Shapouri-Moghaddam A, Mohammadian S, Vazini H, Taghadosi M, Esmaeili SA, Mardani F, et al. Macrophage plasticity, polarization, and function in health and disease. J Cell Physiol 2018;233(9):6425–40.

[8] Zhang Q-Y, Tan J, Huang K, Nie R, Feng Z-Y, Zou C-Y, et al. Polyphenolic-modified cellulose acetate membrane for bone regeneration through immunomodulation. Carbohydr Polym 2023;305:120546.

[9] Bashir S, Sharma Y, Elahi A, Khan F. Macrophage polarization: the link between inflammation and related diseases. Inflamm Res 2016;65(1):1–11.

[10] Tan J, Zhang Q-Y, Song Y-T, Huang K, Jiang Y-L, Chen J, et al. Accelerated bone defect regeneration through sequential activation of the M1 and M2 phenotypes of macrophages by a composite BMP-2@SIS hydrogel: an immunomodulatory perspective. Compos B Eng 2022;243:110149.

[11] Wang Y, Wang J, Gao R, Liu X, Feng Z, Zhang C, et al. Biomimetic glycopeptide hydrogel coated PCL/nHA scaffold for enhanced cranial bone regeneration via macrophage M2 polarization-induced osteo-immunomodulation. Biomaterials 2022;285:121538.

[12] Li M, Sun X, Zhao J, Xia L, Li J, Xu M, et al. CCL5 deficiency promotes liver repair by improving inflammation resolution and liver regeneration through M2 macrophage polarization. Cell Mol Immunol 2020;17(7):753–64.

[13] Wang L, Wang C, Wu S, Fan Y, Li X. Influence of the mechanical properties of biomaterials on degradability, cell behaviors and signaling pathways: current progress and challenges. Biomater Sci 2020;8(10):2714–33.

[14] Zhang XZ, Jiang YL, Hu JG, Zhao LM, Chen QZ, Liang Y, et al. Procyanidins-crosslinked small intestine submucosa: a bladder patch promotes smooth muscle regeneration and bladder function restoration in a rabbit model. Bioact Mater 2021;6(6):1827–38.

[15] Zhang XR, Huang YZ, Gao HW, Jiang YL, Hu JG, Pi JK, et al. Hypoxic preconditioning of human urine-derived stem cell-laden small intestinal submucosa enhances wound healing potential. Stem Cell Res Ther 2020;11(1):150.

[16] Huang LP, Liu Y, Li QJ, Zhang WQ, Wu CY, Zhao LM, et al. A modified small intestinal submucosa patch with multifunction to promote scarless repair and reinvigoration of urethra. Adv Healthcare Mater 2023:e2300519.

[17] He SK, Guo JH, Wang ZL, Zhang Y, Tu YH, Wu SZ, et al. Efficacy and safety of small intestinal submucosa in dural defect repair in a canine model. Mater Sci Eng C 2017;73:267–74.

[18] Song Y-T, Dong L, Hu J-G, Liu P-C, Jiang Y-L, Zhou L, et al. Application of genipin-crosslinked small intestine submucosa and urine-derived stem cells for the prevention of intrauterine adhesion in a rat model. Compos B Eng 2023;250:110461.

[19] Zhang Q-Y, Tan J, Nie R, Song Y-T, Zhou X-L, Feng Z-Y, et al. Acceleration of wound healing by composite small intestinal submucosa hydrogels through immunomodulation. Compos B Eng 2023;254:110550.

[20] Gou M, Huang YZ, Hu JG, Jiang YL, Zhang XZ, Su NC, et al. Epigallocatechin-3-gallate cross-linked small intestinal submucosa for guided bone regeneration. ACS Biomater Sci Eng 2019;5(10):5024–35.

[21] Chu C, Liu L, Wang Y, Wei S, Wang Y, Man Y, et al. Macrophage phenotype in the epigallocatechin-3-gallate (EGCG)-modified collagen determines foreign body reaction. J. Tissue Eng. Regen Med. 2018;12(6):1499–507.

[22] Luo JC, Chen W, Chen XH, Qin TW, Huang YC, Xie HQ, et al. A multi-step method for preparation of porcine small intestinal submucosa (SIS). Biomaterials 2011;32(3):706–13.

[23] Albuquerque N, Neri JR, Lemos M, Yamauti M, de Sousa F, Santiago SL. Effect of polymeric microparticles loaded with catechin on the physicochemical properties of an adhesive system. Operat Dent 2019;44(4). E202-e11.

[24] Sugimoto J, Romani AM, Valentin-Torres AM, Luciano AA, Ramirez Kitchen CM, Funderburg N, et al. Magnesium decreases inflammatory cytokine production: a novel innate immunomodulatory mechanism. J Immunol 2012;188(12):6338–46.

[25] Taghiyar H, Yadollahi B, Kajani AA. Controlled drug delivery and cell adhesion for bone tissue regeneration by Keplerate polyoxometalate (Mo(132))/metronidazole/PMMA scaffolds. Sci Rep 2022;12(1):14443.

[26] Wu M, Han Z, Liu W, Yao J, Zhao B, Shao Z, et al. Silk-based hybrid microfibrous mats as guided bone regeneration membranes. J Mater Chem B 2021;9(8):2025–32.

[27] Badylak SF, Freytes DO, Gilbert TW. Extracellular matrix as a biological scaffold material: structure and function. Acta Biomater 2009;5(1):1–13.

[28] Cao G, Huang Y, Li K, Fan Y, Xie H, Li X. Small intestinal submucosa: superiority, limitations and solutions, and its potential to address bottlenecks in tissue repair. J Mater Chem B 2019;7(33):5038–55.

[29] Xu H, Zhao Q, Song N, Yan Z, Lin R, Wu S, et al. AdipoR1/AdipoR2 dual agonist recovers nonalcoholic steatohepatitis and related fibrosis via endoplasmic reticulum-mitochondria axis. Nat Commun 2020;11(1):5807.

[30] Glynn JJ, Polsin EG, Hinds MT. Crosslinking decreases the hemocompatibility of decellularized, porcine small intestinal submucosa. Acta Biomater 2015;14:96–103.

[31] Chen M, Sun Y, Hou Y, Luo Z, Li M, Wei Y, et al. Constructions of ROS-responsive titanium-hydroxyapatite implant for mesenchymal stem cell recruitment in peri-implant space and bone formation in osteoporosis microenvironment. Bioact Mater 2022;18:56–71.

[32] Rung S, Zhao X, Chu C, Yang R, Qu Y, Man Y. Application of epigallocatechin-3-gallate (EGCG) modified 1-Ethyl-3-(3-dimethylaminopropylcarbodiimide hydrochloride/N-hydroxy-succinimide (EDC/NHS) cross-linked collagen membrane to promote macrophage adhesion. Materials 2021;14(16).

[33] Li R, Zhou C, Chen J, Luo H, Li R, Chen D, et al. Synergistic osteogenic and angiogenic effects of KP and QK peptides incorporated with an injectable and self-healing hydrogel for efficient bone regeneration. Bioact Mater 2022;18:267–83.

[34] Tu C, Lu H, Zhou T, Zhang W, Deng L, Cao W, et al. Promoting the healing of infected diabetic wound by an anti-bacterial and nano-enzyme-containing hydrogel with inflammation-suppressing, ROS-scavenging, oxygen and nitric oxide-generating properties. Biomaterials 2022;286:121597.

[35] Wolf SJ, Melvin WJ, Gallagher K. Macrophage-mediated inflammation in diabetic wound repair. Semin Cell Dev Biol 2021;119:111–8.

[36] Noguchi J, Watanabe S, Nguyen TQ, Kikuchi K, Kaneko H. Development of a lipopolysaccharide (LPS)-supplemented adjuvant and its effects on cell-mediated and humoral immune responses in male rats immunized against sperm. J Reprod Dev 2017;63(1):111–5.

[37] Heng Y, Zhang X, Borggrewe M, van Weering HRJ, Brummer ML, Nijboer TW, et al. Systemic administration of β-glucan induces immune training in microglia. J Neuroinflammation 2021;18(1):57.

[38] Caputa G, Matsushita M, Sanin DE, Kabat AM, Edwards-Hicks J, Grzes KM, et al. Intracellular infection and immune system cues rewire adipocytes to acquire immune function. Cell Metabol 2022;34(5). 747-60.e6.

[39] Etzerodt A, Moestrup SK. CD163 and inflammation: biological, diagnostic, and therapeutic aspects. Antioxidants Redox Signal 2013;18(17):2352–63.

[40] Lucas T, Waisman A, Ranjan R, Roes J, Krieg T, Müller W, et al. Differential roles of macrophages in diverse phases of skin repair. J Immunol 2010;184(7):3964–77.

[41] Han R, Blencke HM, Cheng H, Li C. The antimicrobial effect of CEN1HC-Br against Propionibacterium acnes and its therapeutic and anti-inflammatory effects on acne vulgaris. Peptides 2018;99:36–43.

[42] Zhang J, Fu Y, Yang P, Liu X, Li Y, Gu Z. ROS scavenging biopolymers for anti-inflammatory diseases: classification and formulation. Adv Mater Interfac 2020;7(16):2000632.

[43] Gordon S. Alternative activation of macrophages. Nat Rev Immunol 2003;3(1):23–35.

[44] Gabrusiewicz K, Ellert-Miklaszewska A, Lipko M, Sielska M, Frankowska M, Kaminska B. Characteristics of the alternative phenotype of microglia/

macrophages and its modulation in experimental gliomas. PLoS One 2011;6(8):e23902.
[45] Tan J, Zhang Q-Y, Huang L-P, Huang K, Xie H-Q. Decellularized scaffold and its elicited immune response towards the host: the underlying mechanism and means of immunomodulatory modification. Biomater Sci 2021;9(14):4803–20.
[46] Wang B, Qinglai T, Yang Q, Li M, Zeng S, Yang X, et al. Functional acellular matrix for tissue repair. Mater. Today Bio. 2023;18:100530.
[47] Sicari BM, Dziki JL, Siu BF, Medberry CJ, Dearth CL, Badylak SF. The promotion of a constructive macrophage phenotype by solubilized extracellular matrix. Biomaterials 2014;35(30):8605–12.
[48] Wang X, Chung L, Hooks J, Maestas Jr DR, Lebid A, Andorko JI, et al. Type 2 immunity induced by bladder extracellular matrix enhances corneal wound healing. Sci Adv 2021;7(16).
[49] Wen WC, Kuo PJ, Chiang CY, Chin YT, Fu MM, Fu E. Epigallocatechin-3-gallate attenuates Porphyromonas gingivalis lipopolysaccharide-enhanced matrix metalloproteinase-1 production through inhibition of interleukin-6 in gingival fibroblasts. J Periodontol 2014;85(6):868–75.
[50] Wang X, Xu H, Zhang J. Using personalized 3D printed Titanium sleeve-prosthetic composite for reconstruction of severe segmental bone loss of proximal femur in revision total hip arthroplasty: a case report. Medicine 2020;99(3).
[51] Kielland A, Blom T, Nandakumar KS, Holmdahl R, Blomhoff R, Carlsen H. In vivo imaging of reactive oxygen and nitrogen species in inflammation using the luminescent probe L-012. Free Radic Biol Med 2009;47(6):760–6.
[52] Kong X, Chen H, Li F, Zhang F, Jiang Y, Song J, et al. Three-dimension chitosan hydrogel loading melanin composite nanoparticles for wound healing by anti-bacteria, immune activation and macrophage autophagy promotion. Int J Biol Macromol 2023;237:124176.
[53] Zhang L, Wang X, Cueto R, Effi C, Zhang Y, Tan H, et al. Biochemical basis and metabolic interplay of redox regulation. Redox Biol 2019;26:101284.
[54] Wang Z, Liu Z, Wu C, Liu S, Wang D, Hu C, et al. Computational analysis on antioxidant activity of four characteristic structural units from persimmon tannin. Materials 2022;16(1).
[55] He Y, Yue Y, Zheng X, Zhang K, Chen S, Du Z. Curcumin, inflammation, and chronic diseases: how are they linked? Molecules 2015;20(5):9183–213.
[56] Zhang Q, Huang K, Tan J, Lei X, Huang L, Song Y, et al. Metal-phenolic networks modified polyurethane as periosteum for bone regeneration. Chin Chem Lett 2022;33(3):1623–6.
[57] Torun AN, Kulaksizoglu S, Kulaksizoglu M, Pamuk BO, Isbilen E, Tutuncu NB. Serum total antioxidant status and lipid peroxidation marker malondialdehyde levels in overt and subclinical hypothyroidism. Clin Endocrinol 2009;70(3):469–74.
[58] Capó X, Monserrat-Mesquida M, Quetglas-Llabrés M, Batle JM, Tur JA, Pons A, et al. Hyperbaric oxygen therapy reduces oxidative stress and inflammation, and increases growth factors favouring the healing process of diabetic wounds. Int J Mol Sci 2023;24(8).
[59] Zhang Y, Jin Y, Cui H, Yan X, Fan K. Nanozyme-based catalytic theranostics. RSC Adv 2019;10(1):10–20.
[60] Wei K, Nguyen HN, Brenner MB. Fibroblast pathology in inflammatory diseases. J Clin Invest 2021;(20):131.
[61] Henderson NC, Rieder F, Wynn TA. Fibrosis: from mechanisms to medicines. Nature 2020;587(7835):555–66.
[62] Li L, Ma Y, He G, Ma S, Wang Y, Sun Y. Pilose antler extract restores type I and III collagen to accelerate wound healing. Biomed Pharmacother 2023;161:114510.
[63] Eming SA, Brachvogel B, Odorisio T, Koch M. Regulation of angiogenesis: wound healing as a model. Prog Histochem Cytochem 2007;42(3):115–70.
[64] Gurtner GC, Werner S, Barrandon Y, Longaker MT. Wound repair and regeneration. Nature 2008;453(7193):314–21.
[65] Chakroborty D, Goswami S, Basu S, Sarkar C. Catecholamines in the regulation of angiogenesis in cutaneous wound healing. Faseb J 2020;34(11):14093–102.
[66] DeNardo DG, Ruffell B. Macrophages as regulators of tumour immunity and immunotherapy. Nat Rev Immunol 2019;19(6):369–82.
[67] Liao J, Xu B, Zhang R, Fan Y, Xie H, Li X. Applications of decellularized materials in tissue engineering: advantages, drawbacks and current improvements, and future perspectives. J Mater Chem B 2020;8(44):10023–49.